Effects of temperature on the crystal structure of epidote: a neutron single-crystal diffraction study at 293 and 1070K

Effects of temperature on the crystal structure of epidote: a neutron single-crystal diffraction study at 293 and 1070K

G. Diego Gatta[1,2], Martin Meven [3], Geoffrey Bromiley[4], Alessandro Pavese [1,2]

[1]Dipartimento di Scienze della Terra, Università degli Studi di Milano, Via Botticelli 23, I-20133 Milano Italy

[2]CNR-Istituto per la Dinamica dei Processi Ambientali, Milano, Italy

[3]Forschungsneutronenquelle Heinz Maier-Leibnitz (FRM-II), München, Germany

[4] School of GeoSciences, The University of Edinburgh , UK

Abstract

The effects of temperature on the crystal structure of a natural epidote [$Ca_{1.925}Fe_{0.745}Al_{2.265}Ti_{0.004}Si_{3.037}O_{12}(OH)$, a=8.890(6), b=5.630(4), c=10.150(6)Å and β= 115.36(5)°, Sp. Gr. $P2_1/m$] have been investigated by means of neutron single-crystal diffraction at 293 and 1070K. At room conditions, the structural refinement confirms the presence of Fe^{3+} at the M_3 site [%Fe(M3)=73.1(8)%] and all attempts to refine the amount of Fe at the M(1) site were unsuccessful. Only one independent proton site was located. Two possible hydrogen bonds, with O2 and O4 as acceptors [*i.e.* O(10)–H(1)···O2 and O(10)–H(1)···O4], occur. However, the topological configuration of

the bonds suggests that the O(10)–H(1)···O4 is energetically more favourable, as H(1)···O(4)=1.9731(28)Å, O(10)···O(4)=2.9318(22)Å and O(10)–H(1)···O4=166.7(2)°, whereas H(1)···O(2)=2.5921(23)Å, O(10)···O(2)=2.8221(17)Å and O(10)–H(1)···O2=93.3(1)°. The O(10) - H(1) bond distance corrected for "riding motion" is 0.9943Å. The diffraction data at 1070K show that epidote is stable within the *T*-range investigated, and that its crystallinity is maintained. A positive thermal expansion is observed along all the three crystallographic axes. At 1070K the structural refinement again shows that Fe^{3+} share the M(3) site along with Al^{3+} [$\%Fe(M3)_{1070K}$=74(2)%]. The refined amount of Fe^{3+} at the M(1) is not significant [$\%Fe(M1)_{1070K}$=1(2)%]. The tetrahedral and octahedral bond distances and angles show a slight distortion of the polyhedra at high-*T*, but a significant increase of the bond distances compared to those at room temperature is observed, especially for bond distances corrected for "rigid body motions". The high-*T* conditions affect also the inter-polyhedral configurations: the bridging angle Si(2)-O(9)-Si(1) of the Si_2O_7 group increases significantly with *T*. The high-*T* structure refinement shows that no dehydration effect occurs at least within the *T*-range investigated. The configuration of the H-bonding is basically maintained with temperature. However, the hydrogen bond strength changes at 1070K, as the O(10)···O(4) and H(1)···O(4) distances are slightly longer than those at 293K. The anisotropic displacement parameters of the proton site are significantly larger than those at room condition. Reasons for the thermal stability of epidote up to 1070K observed in this study, the absence of dehydration and/or non-convergent ordering of Al and Fe^{3+} between different octahedral sites and/or convergent ordering on M(3) are discussed.

Keywords: epidote, high-temperature, neutron single-crystal diffraction, structurally incorporated water, hydrogen bonding.

Introduction

Epidotes are a class of sorosilicates with the general formula $A_1A_2M_1M_2M_3(Si_2O_7)(SiO_4)O(OH)$, where the A(1) and A(2) sites with coordination number (CN) >6 and mainly occupied by Ca, and M(1), M(2) and M(3) sites with CN=6 and mainly occupied by Al and Fe^{3+}. However, a large number of elements can substitute Ca at A(1) and A(2) and Al or Fe^{3+} at the M(1) and M(3) sites, making the

crystal chemistry of natural epidote more complex (Franz and Liebsher 2004). According to the Commission of the International Mineralogical Association, the term "epidote" *sensu stricto* (s.s.) should be used for members with composition $Ca_2Al_2Fe^{3+}Si_3O_{12}(OH)$. In Nature, epidotes s.s. usually form during low grade metamorphism and hydrothermal activity (250–400°C, 1-2 kbars). However, they are stable over a wide range of pressure and temperature in continental and oceanic crust (Poli and Schmidt 1998). Magmatic epidote has been also found (Schmidt and Poli 2004). The stability of epidotes s.s. depends not only on pressure and temperature, but is also significantly influenced by the Al/Fe^{3+} ratio, oxygen fugacity, fluid composition and solution pH (Holdaway 1972, Liou 1973, Bird and Helgeson 1980, Bird et al. 1988, Klemd 2004). Epidote s.s. is particulary common in metamorphosed basalts and gabbros where it replaces plagioclase, pyroxene and olivine. It can also be found in schists and marbles. In addition, it is frequently found infilling vugs or veins in these rocks. Epidotes are commonly associated with chlorite, actinolite and quartz.

Epidote s.s. is metrically monoclinic and the unit-cell constants appear to be correlated to the amount of Fe^{3+} (unit-cell $8.861<a<8.922$, $5.577<b<5.663$, $10.140<c<10.200$Å, $115.31<\beta<115.93^{o}$, Z=2, Franz and Liebsher 2004). The space group is $P2_1/m$; however possible symmetry reduction to Pm, $P2_1$ *or* $P\bar{1}$, due to cation ordering, have been reported (Franz and Liebsher 2004). Epidote is a structurally complex mineral having both single silicate tetrahedrons, SiO_4, and double silicate tetrahedrons, Si_2O_7. Continuous chains of AlO_6 and $AlO_4(OH)_2$ octahedra running parallel to the *b*-axis and are bridged by single SiO_4 and double Si_2O_7 tetrahedral groups (Fig. 1). These chains are arranged in parallel planes and the perfect cleavage breaks the bonds between these planes. The formula of a chemically simple epidote s.s. can be expressed in a such a way so as to reflect this organization: $^{A1}Ca^{A2}Ca^{M1}(Al,Fe^{3+})^{M2}(Al)^{M3}(Al,Fe^{3+})O(SiO_4)(Si_2O_7)(OH)$. Several studies based on different techniques, recently reviewed by Franz and Liebsher (2004), showed a preference of Fe^{3+} for M(3) and M(1) sites. The replacement of Al by Fe^{3+} in the epidote structure does not significantly exceed one atom per formula unit [*i.e.* the composition lies between $Ca_2Al_3Si_3O_{12}(OH)$ and $Ca_2Fe^{3+}Al_2Si_3O_{12}(OH)$].

Several authors have investigated the crystal structure and crystal chemistry of compositionally different epidotes s.s. at room or low-temperature by means of X-ray and neutron single-crystal diffraction, IR and Mössbauer spectroscopy and theoretical

models (among those: Ito et al. 1954, Hanisch and Zemann 1966, Dollase 1968, 1969, 1971, 1973; Gabe et al. 1973, Langer and Raith 1974, Nozik et al. 1978, Bird and Helgeson 1980, Carbonin and Molin 1980, Stergiou et al. 1987, Bird et al. 1988, Kvick et al. 1988, Bonazzi and Menchetti 1995, Comodi and Zanazzi 1997, Giuli et al. 1999) and recently reviewed by Bonazzi and Menchetti (2004), Franz and Liebsher (2004) and Liebsher (2004). However, no study has been devoted to the high-temperature behaviour of epidote s.s. based on in-situ high-temperature (H*T*) experiments, despite the importance of this minerals in the field of the metamorphic and/or magmatic petrology. The only in-situ H*T* X-ray single-crystal diffraction study was performed on a Sr-piemontite by Catti et al. (1988), although the X-ray diffraction study proved to be insufficient to monitor *T*-induced disordering phenomena and to locate directly the proton site at H*T* in epidote (Catti et al. 1988). In this light, the aim of the present study is a re-investigation of the crystal structure and H*T* crystal chemistry of a natural epidote s.s. at ambient and high-temperature (up to 1070K) by means of single-crystal neutron diffraction, in order to define (1) the *T*-induced structure evolution and the mean deformation mechanisms, (2) any possible *T*-induced disordering phenomena ($Al \leftrightarrow Fe^{3+}$), and (3) any change in hydrogen bonding or dehydration effects. Neutron diffraction is the best technique for a study of partial site-occupancy by Fe and Al, since the neutron-scattering lengths of these two elements are significantly different (*i.e.* b_{56Fe}=9.94 and b_{Al}=3.449 fm). In addition, the independence of scattering lengths and $(\sin\theta)/\lambda$ allows a separation of substitutional and thermal-motion effects.

Experimental methods

A natural, dark-green, gem-quality single-crystal of epidote s.s. (~ 2.4 cm^3) from the intrusive/metamorphic complex of Val Sissone, Valmalenco (Rhetic Alps, Italy) was used in this study. The sample and the chemical analysis [$Ca_{1.925}Fe_{0.745}Al_{2.265}Ti_{0.004}Si_{3.037}O_{12}(OH)$, in Bedognè et al. 1993] have been kindly provided by Museo di Storia Naturale, Milano, Italy.

A fragment of the crystal of approximately 2.3 x 2.5 x 4 mm^3 was selected for the neutron diffraction experiment. Under a polarised microscope, the crystals appeared free of defects, twinning or zoning. A preliminary test of the crystal was performed by means of X-ray diffraction at the Earth Science Department –

University of Milano using an Xcalibur-1 Oxford Diffraction diffractometer equipped with CCD, with monochromatized Mo-*K*α radiation. Accurate cell parameters were measured using diffraction data from a small fragment of about 0.1 x 0.1 x 0.1 mm, within the range $5^\circ<2\theta<40^\circ$, giving a metrically monoclinic lattice with: a=8.8900(3)Å, b=5.6286(2) Å, c=10.1558(4)Å, β=115.412(2)° and V=459.02(4)Å^3. The single-crystal neutron diffraction experiment was first performed at room temperature with the four-circle diffractometer HEiDi (beam line SR9) at the FRM-II reactor (Forschungsneutronenquelle Heinz Maier-Leibnitz) at Garching (near München), Germany. The FRM II provides a maximum undisturbed thermal neutron flux density of $8x10^{14}cm^{-2}s^{-1}$ at a nominal thermal power of 20MW. The incident radiation (CW with λ=0.5500Å) was obtained using a focusing Cu-(420) monochromator. Cu monochromator cystals show typically a strong λ/2 contamination; therefore, a neutron filter (0.5 mm Hf foil) was used to cut off the neutrons around the λ/2 area from the neutron spectrum. An integrated slit system defined the cross section of the entrance window of the detector. A ^{3}He single counter detector was used [Eurisys 73NH17/5X end window counter, 50 mm entrance window, 5 bar ^{3}He pressure and 170 mm active length for high detection probability (>90% at 0.8 Å), separation of γ radiation by pulse height discrimination]. The unit-cell parameters refined on the basis of the 37 Bragg reflections at T=293K are: a=8.890(6)Å, b=5.630(4)Å, c=10.150(6)Å, β=115.36(5)°. A total number of 2741 reflections were recorded with $-16\leq h \leq 12$, $0\leq k \leq 10$ and $0\leq l \leq 18$ (maximum 2θ = 60°, $\sin(\theta)/\lambda\sim0.9$). Two standard reflections were measured with every 450 min throughout the experiment and the intensity variation was within σ(I). Further details of the data collection are reported in Table 1. The systematic extinction rules agreed with the space group $P2_1/m$. Diffraction data were then corrected for Lorentz effect. No absorption correction was applied because of the shape and the dimensions of the sample. After correction, the discrepancy factor for the symmetry related reflections (Laue class: 2/m) was R_{int} = 0.0357.

A further set of data was collected at T=1070 K, using an air cooled furnace designed at the Jülich Centre for Neutron Science (JCNS) (temperature precision: ± 1K). The temperature of the crystal was slowly increased (~200K/h) and kept at T=1070K for 3 hours prior to data collection. Unit-cell parameters refined on the basis of the 37 Bragg reflections at 1070K are: a=8.939(10)Å, b=5.682(10)Å,

c=10.251(4)Å and β= 115.78(5)°. A total of 841 reflections were recorded with -13≤ h ≤0, 0≤k ≤8 and -15≤ l ≤15 (maximum 2θ=52°, sin(θ)/λ~0.8) (Table 1). The lower number of reflections compared to 293K are due to the shadowing effect of the furnace and to a technical problem at the beam-line. As with data collection at room temperature, two standard reflections were measured every 450 min throughout the experiment and the intensity variation was within σ(I). Further details of the data collection are reported in Table 1. The systematic extinction rules agreed with the space group $P2_1/m$. Diffraction data were then corrected for Lorentz effect and no absorption correction was applied. After correction, the discrepancy factor for the symmetry related reflections was R_{int} = 0.071.

Structure refinements

The neutron diffraction data of epidote collected at room temperature were first processed with the program E-STATISTICS, implemented in the WinGX package (Farrugia 1999). The statistics of distributions of the normalized structure factors (E's) showed that the structure is centrosymmetric at 65.4% likelihood. The Sheldrick's $|E^2-1|$ criterion (Sheldrick 1997) indicated that the structure is centrosymmetric ($|E^2-1| = 0.891$) (Table 1). The intensity data were then processed with the program ASSIGN-SPACEGROUP (in WinGX, Farrugia 1999), aimed to check the supposed symmetry by comparing the equivalent reflections. The program selected two possible space groups (both belonging to the 2/m Laue class): $P2_1$ and $P2_1/m$. The Combined Figure of Merit (CFOM) showed that the centrosymmetric space group $P2_1/m$ is highly likely (CFOM - $P2_1/m$ = 2.367, CFOM- $P2_1$ =4.163; the lower the value of CFOM, the more likely the assignment is correct) (Table 1). The crystal structure refinement was then performed in the space group $P2_1/m$ using the SHELX-97 software (Sheldrick 1997), with anisotropic thermal displacement parameters and starting from the atomic coordinates of Kvick et al. (1988), with a H-free structural model. The neutron scattering lengths of Ca, Al, Fe, Si, O and H have been used according to Sears (1986). The secondary isotropic extinction effect was corrected according to Larson's formalism (1970), as implemented in the SHELXL-97 package (Sheldrick 1997). When convergence was achieved, one intense negative residual peaks (~ -25 fm/Å^3) at x~0.05, y=1/4, z~0.32 (~0.98Å from the oxygen site O10) was found in the final difference-Fourier map of the nuclear density (Fig. 2). As the

neutron scattering length of hydrogen is negative (-3.7409 fm/Å^3), a further refinement was then performed assigning H to the residual peak, with anisotropic thermal parameters for all sites including the proton site. Convergence was rapidly achieved and all the principal mean square atomic displacement parameters were positively defined. The variance-covariance matrix showed no significant correlation among the refined parameters. At the end of the last cycle of refinement, no peak larger than +1.07/-1.04 fm/Å^3 was present in the final difference-Fourier map of the nuclear density (Fig. 2, Table 1). The final agreement index (R_1) was 0.0351 for 127 refined parameters and 1756 unique reflections with Fo>4σ(Fo) (Table 1). Site positions are reported in Table 2a, displacement parameters in Tables 3a and 4a. Relevant bond lengths and angles are listed in Tables 5a.

The neutron diffraction data collected at 1070K were processed following the same protocol already adopted for the refinement at room temperature. The preliminary data treatment on the symmetry of the structure showed that the structure is centrosymmetric at 53% likelihood ($|E^2-1| = 0.846$), and the CFOM of the $P2_1$ and $P2_1/m$ are similar, showing that there is not a clear evidence of the presence of the inversion center (Table 1). The anisotropic structural refinement was performed starting from the structural model previously refined at room condition. When convergence was achieved, no peak larger than +1.15/-1.21 fm/Å^3 was present in the difference-Fourier map of the nuclear density (Table 1). At the end of the refinement, an inspection of the variance-covariance matrix showed no significant correlation among the refined parameters. All the principal mean square atomic displacement parameters were positively defined. The final agreement index (R_1) was 0.0548 for 126 refined parameter and 519 unique reflections with Fo>4σ(Fo) (Table 1). The refined atomic positions at 1070K are reported in Table 2b, the displacement parameters in Table 3b and 4b. Bond lengths and angles are listed in Tables 5b. A further isotropic structure refinement was performed, increasing significantly the observation/refined parameters ratio. The refined atomic positions and the occupancy factors of Fe and Al at the octahedral sites agree with those obtained from the anisotropic refinement within the *e.s.ds*, proving the reliability of the anisotropic structure refinement at 1070K.

Discussion and conclusions

This is the first experiment in which the structural evolution of epidote in response to the temperature is described on the basis of in-situ neutron diffraction data.

At room conditions, the structural refinement confirms the presence of Fe^{3+} at the M_3 site [%Fe(M3)=73.1(8)%] (Table 2a). Any attempt to refine the amount of Fe at the M(1) site was unsuccessful; in other words, the M(1) site is completely occupied by Al, whereas Fe and Al occupy the M(3) site (Table 2a). This is in agreement with the previous results of Bonazzi and Menchetti (1995), who found that a significant amount of Fe^{3+} is found at the M(1) site only when the volume of the M(3) polyhedron is higher than 11Å^3. As the refined volume of the M(3) polyhedron approaches 11Å^3 (Table 5a), we cannot expect a significant amount of Fe^{3+} at the M(1) site. The refined amount of Fe on the basis of the neutron structural refinement is in good agreement with the chemical analysis [*i.e.* 0.735 *vs* 0.745 a.p.f.u.]. According to the previous studies (Franz and Liebsher 2004 and references therein), the M(2) site was found to be occupied only by Al. The structural refinement at room temperature shows that the thermal displacement ellipsoids are only slightly pronounced (Table 3a and 4a). The largest anisotropy is observed for the O(3), O(8) and O(9) oxygen sites, with R1/R3~2 (where R1 and R3 represent the longest and the shortest root-mean-square components of the thermal ellipsoids, respectively; Table 4a). A similar finding was reported by Kvick et al. (1988), who suggested this effect is driven by rotation of the Si(2)-tetrahedron due to the presence of Fe^{3+} at the M(3) site with respect to a Fe-free structure (*i.e.* zoisite, Smith et al. 1987). The least-square refinement shows that there is only one independent proton site in the epidote structure and its refined position is in good agreement with that of Kvick et al. (1988). Two possible hydrogen bonds, with O2 and O4 as acceptors [*i.e.* O(10)–H(1)···O2 and O(10)–H(1)···O4, Table 5a], occur. However, the topological configuration of the bonds suggests that the O(10)–H(1)···O4 is energetically more favourable, as H(1)···O(4)=1.9731(28)Å, O(10)···O(4)=2.9318(22)Å and O(10)–H(1)···O4=166.7(2)°, whereas H(1)···O(2)=2.5921(23)Å, O(10)···O(2)=2.8221(17)Å and O(10)–H(1)···O2=93.3(1)°. Evidence of possible hydrogen bonds with O(2) as acceptors, with a complex bifurcated configuration, where reported in previous IR-spectroscopy studies (Liebscher et al. 2002, Liebsher 2004). The O(10) - H(1) bond distance corrected for “riding motion” (Busing and

Levy 1964) is 0.9943Å (Table 5a). Kvick et al. (1988), on the basis of the structural refinement of epidote s.s. at 15K, suggested that the deviation of the O(10) – H(1)···O4 angle from the linearity (*i.e.* 180°) might be ascribable to the electrostatic repulsion from the trivalent cations at the M(3)-site and from the Ca(2)-site, as M(3)···H(1)~2.728 and Ca(2)···H(1)~3.004Å. In our refinement at 298K we obtain: M(3)···H1~2.782Å and Ca(2)···H(1)~3.014Å, reflecting a possible repulsion effect. The almost linear hydrogen bond in zoisite at 15K [a Fe-free epidote, in which O(10)–H(1)···O4 = 176.4(2)° , O(10)···O(4) = 2.742(2)Å and H(1)···O(4) = 1.752(2), Smith et al. 1987], suggests that the presence of Fe^{3+} at the M(3)-site leads to a weakening of the bonds, as shown by the increase of the O(10)···O(4) and H(1)···O(4) distances. This agrees with some experimental findings based on vibrational spectroscopy in which the O-H stretch frequencies were found to be positively correlated with Fe content (Langer and Raith 1974; Liebscher 2004): the higher the Fe amount into the structure, the higher the O-H stretching frequency. The comparative study of Franz and Liebscher (2004), based on a wide numbers of structure refinements of epidotes s.s. with different Fe-content, shows a significant increase of the O(10)···O(4) value with increasing the Fe-content.

The diffraction data at 1070K show that epidote s.s. is stable within the *T*-range investigated and that its crystallinity is maintained. This result is in agreement with previous experimental findings on Sr-piemontite, which shows a structural break down at about 1150K (Catti et al. 1988). However, the crystal chemistry of epidote s.s. and that of Sr-piemontite are significantly different. A positive thermal expansion is observed along all the three crystallographic axes of our epidote s.s. ($\Delta a/a \approx 0.55\%$, $\Delta b/b \approx 0.91\%$, $\Delta c/c \approx 1.00\%$ and $\Delta V/V \approx 2.4\%$ with ΔT=777K). As observed at room conditions, the 1070K the structure refinement also shows that Fe^{3+} shares the M(3) site along with Al^{3+} [$\%Fe(M3)_{1070K}$=74(2)%] (Table 2b). The refined amount of Fe^{3+} at the M(1) site is not significant [$\%Fe(M1)_{1070K}$=1(2)%] (Table 2b). The tetrahedral and octahedral bond distances and angles show a slight distortion of the polyhedra at high-*T*, but a significant increase of the bond distances compared to those at room temperature is observed, especially for bond distances corrected for “rigid body motions” following Downs et al. (1992) and Downs (2000) (Table 5b). The H*T*-conditions also affect the inter-polyhedral configurations: the bridging angle Si(2)-O(9)-Si(1) of the Si_2O_7 group, for example, increases significantly from 154.59(9)° at

298K to 157.4(5)° at 1070K, respectively (Tables 5a and 5b). The high-*T* structural refinement shows that no dehydration effect occurs at least within the *T*-range investigated. The configuration of the H-bonding is basically maintained with temperature, as shown by the bond distances and angles reported in Table 5b. However, the hydrogen bond strength changes at 1070K, as the O(10)···O(4) and H(1)···O(4) distances are slightly longer than those at 293K. The anisotropic displacement parameters of the proton site are significantly larger than those at room condition, although the R1/R3 ellipticity ratios are similar (Tables 4b). On the whole, the structure reacts in response to the applied temperature without any drastic change, but mainly by increasing inter-atomic bond distances and thermal vibration of all the atomic sites, as shown in Fig. 3, and with inter-polyhedral tilting.

The thermal stability of epidote s.s. up to 1070K observed in this study, the absence of dehydration and/or non-convergent ordering of Al and Fe^{3+} between different octahedral sites and/or convergent ordering on M(3) (Fehr and Heuss-Assbichler 1997, Franz and Liebscher 2004 and references therein, Gottschalk 2004 and references therein) are likely due to the slow kinetics of the aforementioned processes. Fehr and Heuss-Assbichler (1997) studied the kinetics of the non-convergent ordering process of Al and Fe^{3+} between M(3) and M(1) sites, heating epidote with different Fe-content at 773, 873, and 923K (at 0.3 GPa) for 1 to 22 days under controlled oxygen fugacity. The experiments showed that after 5 days equilibrium was achieved (Fehr and Heuss-Assbichler 1997). A large crystal, as that used for this neutron diffraction experiment, and the short time of the in-situ high-*T* experiment likely hindered the aforementioned *T*-induced processes.

Acknowledgements

The authors thank the Forschungsneutronenquelle Heinz Maier-Leibnitz (FRM-II), München, Germany, for the allocation of neutron beam time. This work was also funded by the Italian Ministry of University and Research, MIUR-Project: 2006040119_004.

References

Bedognè F., Montrasio A., Sciesa E. (1993) Valmalenco – I minerali della provincia di Sondrio. Bettini, Sondrio (Italy), 275 p.

Bird, D.K. and Helgeson, H.C. (1980) Chemical interaction of aqueous solutions with epidote-feldspar mineral assemblages in geologic systems, I: thermodynamic analysis of phase relations in the system CaO-FeO-Fe_2O_3-Al_2O_3-SiO_2-H_2O-CO_2. Am J Science 280:907–941.

Bird, D.K., Cho, M., Janik, C.J., Liou, J.G., and Caruso, L.J. (1988) Compositional, order-disorder, and stable isotopic characteristics of Al-Fe epidote, state 2–14 drill hole, Salton Sea geothermal system. J Geophys Res 93(B11):13135-13144.

Bonazzi P, Menchetti S (1995) Monoclinic members of the epidote group: Effect of the $Al \leftrightarrow Fe^{3+} \leftrightarrow Fe^{2+}$ substitution and of the entry of REE^{3+}. Mineral Petrol 53:133-153.

Bonazzi P, Menchetti S (2004) Manganese in monoclinic members of the epidote group: piemontite and related minerals. In G. Franz and A. Liebscher, Eds., Epidotes, Vol. 56, p. 495-552. Reviews in Mineralogy and Geochemistry, Mineralogical Society of America and Geochemical Society, Washington, U.S.A.

Busing WR, Levy HA (1964) The effect of thermal motion on the estimation of bond lengths from diffraction measurements. Acta Cryst 17:142-146.

Carbonin S, Molin G (1980) Crystal-chemical considerations of eight metamorphic epidotes. N Jb Mineral Abh 139:205-215.

Catti M, Ferraris G, Ivaldi G (1988) Thermal behaviour of the crystal structure of strontian piemontite. Am Mineral 73:1370-1376.

Comodi P, Zanazzi PF (1997) The pressure behaviour of clinozoisite and zoisite. An X-ray diffraction study. Am Mineral 82:61-68.

Dollase WA (1968) Refinement and comparison of the structures of zoisite and clinozoisite. Am Mineral 53:1882-1898.

Dollase WA (1969) Crystal structure and cation ordering of piemontite. Am Mineral 54:710-17.

Dollase WA (1971) Refinement of the crystal structure of epidote, allanite and hancockite. Am Mineral 56:447-464.

Dollase WA (1973) Mössbauer spectra and iron distribution in the epidote-group minerals. Z Kristallogr 138:41–63.

Downs RT (2000) Analysis of harmonic displacement factors. In R.M. Hazen and R.T. Downs, Eds., High-Temperature and High-Pressure Crystal Chemistry, Vol. 41, p. 61-117. Reviews in Mineralogy and Geochemistry, Mineralogical Society of America and Geochemical Society, Washington, U.S.A.

Downs RT, Gibbs GV, Bartelmehs KL, Boisen Jr.MB (1992) Variations of bond lengths and volumes of silicate tetrahedra with temperature. Am Mineral 77:751-757.

Farrugia LJ (1999) WinGX suite for small-molecule single-crystal crystallography. J Appl Crystallogr 32:837-838.

Fehr KT, Heuss-Assbichler (1997) Intracrystalline equilibria and immiscibility gap along the join clinozoisite-epidote: An experimental and ^{57}Fe Mössbauer study. N Jb Mineral Abh 172:43-67.

Franz G, Liebscher A (2004) Physical and chemical properties of epidote minerals – An Introduction. In G. Franz and A. Liebscher, Eds., Epidotes, Vol. 56, p. 1-81. Reviews in Mineralogy and Geochemistry, Mineralogical Society of America and Geochemical Society, Washington, U.S.A.

Gabe EJ, Portheine FC, Whitlow SH (1973) A reinvestigation of the epidote structure: confirmation of the iron location. Am Mineral 58:218-223.

Giuli G, Bonazzi P, Menchetti S (1999) Al-Fe disorder in synthetic epidotes: a single-crystal X-ray diffraction study. Am Mineral 84:933-936.

Gottschalk M (2004) Thermodynamic properties of zoisite, clinozoisite and epidote. In G. Franz and A. Liebscher, Eds., Epidotes, Vol. 56, p. 83-124. Reviews in Mineralogy and Geochemistry, Mineralogical Society of America and Geochemical Society, Washington, U.S.A.

Hanisch K, Zemann J (1966) Messung des Ultrarot-Pleochroismus von Mineralen. IV. Der Pleochroismus der OH-Streckfrequenz in Epidot. N Jb Mineral Mon 1966:19-23.

Holdaway MJ (1972) Thermal stability of Al-Fe epidotes as a function of fO_2 and Fe content. Contrib Min Petrol 37:307–340.

Liou JG (1973) Synthesis and stability relations of epidote, $Ca_2Al_2FeSi_3O_{12}(OH)$. J Petrol 14:381–413.

Ito T, Morimoto N, Sadanga R (1954) On the structure of epidote. Acta Cryst 7:53-59.

Klemd R (2004) Fluid inclusions in epidote minerals and fluid development in epidote-bearing rocks. In G. Franz and A. Liebscher, Eds., Epidotes, Vol. 56, p. 197-234. Reviews in Mineralogy and Geochemistry, Mineralogical Society of America and Geochemical Society, Washington, U.S.A.

Kvick Å, Pluth JJ, Richardson Jr. JW, Smith JV (1988) The ferric ion distribution and hydrogen bonding in epidote: a neutron diffraction study at 15 K. Acta Cryst B44:351-355.

Langer K, Raith M (1974) Infrared spectra of Al-Fe(III)-epidotes and zoisites $Ca_2(Al_{1-p}Fe^{3+}_p)Al_2O(OH)[Si_2O_7][SiO_4]$. Am Mineral 59:1249-1258.

Larson AC (1970) Crystallographic Computing. F. R. Ahmed, S. R. Hall and C. P. Huber, Eds., Copenhagen, Denmark, Munksgaard., pp. 291 – 294.

Liebscher A (2004) Spectroscopy of epidote minerals. In G. Franz and A. Liebscher, Eds., Epidotes, Vol. 56, p. 125-170. Reviews in Mineralogy and Geochemistry, Mineralogical Society of America and Geochemical Society, Washington, U.S.A.

Liebscher A, Gottschalk M, Franz G (2002) The substitution Fe^{3+}-Al and the isosymmetric displacive phase stransition in synthetic zoisite: A powder X-ray and infrared spectroscopy study. Am Mineral 87:909-921.

Nozik YK, Kanepit VN, Fykin LY, Makarov YS (1978) A neutron diffraction study of the structure of epidote. Geochem Int 15:66-69.

Poli S, Schmidt MW (2004) Experimental subsolidus studies on epidote minerals. In G. Franz and A. Liebscher, Eds., Epidotes, Vol. 56, p. 171-195. Reviews in Mineralogy and Geochemistry, Mineralogical Society of America and Geochemical Society, Washington, U.S.A.

Robinson K, Gibbs GV, Ribbe PH (1971) Quadratic Elongation: A Quantitative Measure of Distortion in Coordination Polyhedra. Science 172:567-570.

Sears V.F. (1986) Neutron Scattering Lengths and Cross-Sections. In K. Sköld and D.L. Price, Eds., Neutron Scattering, Methods of Experimental Physics, Vol. 23A, p. 521-550. Academic Press, New York.

Sheldrick GM (1997) SHELX-97. Programs for crystal structure determination and refinement. University of Göttingen, Germany.

Schmidt MW, Poli S (2004) Magmatic epidotes. In G. Franz and A. Liebscher,

Eds., Epidotes, Vol. 56, p. 399-430. Reviews in Mineralogy and Geochemistry, Mineralogical Society of America and Geochemical Society, Washington, U.S.A.

Smith JV, Pluth JJ, Richardson Jr. JW, Kvick Å (1988) Neutron diffraction study of zoisite at 15 K and X-ray study at room temperature. Z Kristallogr 179:305-321.

Stergiou AC, Rentzeperis PJ, Sklavounos S (1987) Refinement of the crystal structure of a medium iron epidote. Z. Kristallogr 178:297-305.

Tables and Figures

Table 1. Details pertaining to the data collection and refinement of epidote at 298 and 1073K.

Crystal size (mm^3)	2.3 x 2.5 x 4	2.3 x 2.5 x 4
Cell parameters	a = 8.890(6)Å	a = 8.939(10) Å
	b = 5.630(4)Å	b = 5.682(10)Å
	c = 10.150(6)Å	c = 10.251(4)Å
	β= 115.36(5)°	β= 115.78(5)°
Z	2	2
T (K)	298	1070
Radiation (Å)	0.5500	0.5500
Scan type, steps and width:		
2θ <60°	31 steps, pure ω-scan	31 steps, pure ω-scan
Time per step (s)	5	5
u, v, w	5.4, -12.0, 16.3	5.4, -12.0, 16.3
Max. 2θ (°)	60	52
	-16≤ h ≤12	-13≤ h ≤0
	0≤ k ≤10	0≤ k ≤8
	0≤ l ≤18	-15≤ l ≤15
No. measured reflections	2741	841
Space Group assignment :		
Prob. centrosymmetric structure	65.4%	53.0%
$\lvert E^2-1 \rvert$	0.891	0.846
CFOM- $P2_1/m$	2.367	7.329
CFOM- $P2_1$	4.163	6.831
Selected space group	$P2_1/m$	$P2_1/m$
No. unique refl. with F_o >4σ(F_o)	1756	519
No. refined parameters	127	127
Extinction correction factor	0.017(1)	0.013(4)
R_{int}	0.0357	0.0710
R_1 (F) with F_o >4σ(F_o)	0.0351	0.0548
wR_2 (F^2)	0.0486	0.0922
GooF	1.001	1.139
Weighting Scheme: a, b	0.01, 0	0.01, 1
Residuals (fm/ $Å^3$)	+1.07/-1.04	+1.16/-1.21

Note: $R_{int} = \Sigma \mid F_{obs}^2 - F_{obs}^2(\text{mean}) \mid / \Sigma [F_{obs}^2]$; $R_1 = \Sigma(|F_{obs}| - |F_{calc}|)/\Sigma|F_{obs}|$;
$wR_2 = [\Sigma[w(F^2_{obs} - F^2_{calc})^2]/\Sigma[w(F^2_{obs})^2]]^{0.5}$;
$w = 1/ [\sigma^2(F_{obs}^2) + (a*P)^2 + b*P]$; $P = (\text{Max}(F_{obs}^2, 0) + 2*F_{calc}^2)/3$;
ω-scan width = $(u + v*\tan\theta + w*\tan^2\theta)^{0.5}$

Table 2a. Refined fractional atomic coordinates and equivalent isotropic temperature factors (Å^2), with standard deviations in parentheses, based on the diffraction data collected at 293K.

Site	*x/a*	*y/b*	*z/c*	U_{eq}
CA(1)	0.75755(12)	0.75	0.15178(12)	0.0088(1)
CA(2)	0.60525(12)	0.75	0.42409(13)	0.0111(1)
SI(1)	0.33936(10)	0.75	0.04749(11)	0.0036(1)
SI(2)	0.68410(11)	0.25	0.27477(11)	0.0041(1)
SI(3)	0.18396(10)	0.75	0.31832(11)	0.0037(1)
M(1)	0	0	0	0.0036(2)
M(2)	0	0	0.5	0.0041(1)
M(3)	0.29382(6)	0.25	0.22428(6)	0.0049(1)
O(1)	0.23406(5)	-0.00563(8)	0.04145(6)	0.0065(1)
O(2)	0.30384(6)	-0.01778(8)	0.35522(6)	0.0069(1)
O(3)	0.79461(6)	0.01389(8)	0.33999(6)	0.0082(1)
O(4)	0.05280(8)	0.25	0.12950(9)	0.0049(1)
O(5)	0.04160(8)	0.75	0.14566(9)	0.0051(1)
O(6)	0.06664(8)	0.75	0.40667(9)	0.0055(1)
O(7)	0.51529(8)	0.75	0.18079(10)	0.0082(1)
O(8)	0.52467(9)	0.25	0.30785(11)	0.0117(1)
O(9)	0.62773(12)	0.25	0.09900(11)	0.0139(1)
O(10)	0.08212(9)	0.25	0.42841(9)	0.0058(1)
H(1)	0.0537(2)	0.25	0.3242(2)	0.0194(3)
Note: %Al[M(1)]=99.9(6)% and %Fe[M(1)]=0.1(6); %Al[M(2)]=100%; %Al[M(3)]=26.9(8)% and %Fe[M(3)]= 73.1(8)%				

Table 2b. Refined fractional atomic coordinates and equivalent isotropic temperature factors (Å^2), with standard deviations in parentheses, based on the diffraction data collected at 1070K.

Site	*x/a*	*y/b*	*z/c*	U_{eq}
CA(1)	0.7588(9)	0.75	0.1535(8)	0.030(2)
CA(2)	0.6002(9)	0.75	0.4183(8)	0.036(2)
SI(1)	0.3385(6)	0.75	0.0440(7)	0.013(1)
SI(2)	0.6832(6)	0.25	0.2728(7)	0.012(1)
SI(3)	0.1840(6)	0.75	0.3184(7)	0.012(2)
M(1)	0	0	0	0.014(2)
M(2)	0	0	0.5	0.014(1)
M(3)	0.2934(4)	0.25	0.2257(4)	0.020(1)
O(1)	0.2334(3)	-0.0087(8)	0.0384(3)	0.022(1)
O(2)	0.3039(3)	-0.0187(8)	0.3555(4)	0.022(1)
O(3)	0.7935(4)	0.0157(8)	0.3409(4)	0.024(1)
O(4)	0.0562(6)	0.25	0.1276(5)	0.016(1)
O(5)	0.0442(6)	0.75	0.1471(6)	0.018(1)
O(6)	0.0665(6)	0.75	0.4057(6)	0.017(1)
O(7)	0.5123(6)	0.75	0.1769(6)	0.027(1)
O(8)	0.5221(6)	0.25	0.3032(6)	0.029(1)
O(9)	0.6331(8)	0.25	0.1018(6)	0.039(1)
O(10)	0.0810(7)	0.25	0.4296(8)	0.021(1)
H(1)	0.0579(14)	0.25	0.3299(13)	0.045(3)
Note: %Al[M(1)]=99(2)% and %Fe[M(1)]=1(2)%; %Al[M(2)]=100%; %Al[M(3)]=26(2)% and %Fe[M(3)]=74(2)%				

Table 3a. Refined displacement parameters (Å^2) in the expression: $-2\pi^2[(ha^*)^2U_{11} + \ldots + 2hka^*b^*U_{12} + \ldots + 2klb^*c^*U_{23}]$, based on the data collected at 293K. *Ueq* is defined as one third of the trace of the orthogonalised *Uij* tensor.

Site	U_{11}	U_{22}	U_{33}	U_{12}	U_{13}	U_{23}
CA(1)	0.0118(3)	0.0083(3)	0.0086(4)	0	0.0066(3)	0
CA(2)	0.0099(3)	0.0161(3)	0.0068(3)	0	0.0031(3)	0
SI(1)	0.0030(3)	0.0035(2)	0.0038(3)	0	0.0011(3)	0
SI(2)	0.0046(3)	0.0041(2)	0.0038(3)	0	0.0018(3)	0
SI(3)	0.0031(2)	0.0036(2)	0.0043(3)	0	0.0016(3)	0
M(1)	0.0036(4)	0.0028(3)	0.0044(4)	-0.0003(3)	0.0017(3)	-0.0003(3)
M(2)	0.0043(3)	0.0028(3)	0.0054(4)	0.0003(3)	0.0022(3)	0.0001(3)
M(3)	0.0034(2)	0.0053(2)	0.0056(2)	0	0.0015(2)	0
O(1)	0.0052(1)	0.0045(1)	0.0100(2)	0.0011(1)	0.0034(1)	0.0008(1)
O(2)	0.0064(1)	0.0067(1)	0.0075(2)	-0.0007(1)	0.0028(1)	-0.0026(1)
O(3)	0.0064(1)	0.0044(1)	0.0092(2)	0.0007(1)	-0.0009(2)	-0.0009(1)
O(4)	0.0050(2)	0.0045(2)	0.0048(3)	0	0.0017(2)	0
O(5)	0.0054(2)	0.0050(2)	0.0043(2)	0	0.0014(2)	0
O(6)	0.0073(2)	0.0044(2)	0.0073(3)	0	0.0055(2)	0
O(7)	0.0053(2)	0.0099(2)	0.0073(3)	0	0.0006(2)	0
O(8)	0.0100(3)	0.0144(3)	0.0153(4)	0	0.0099(3)	0
O(9)	0.0183(3)	0.0197(3)	0.0063(3)	0	0.0077(3)	0
O(10)	0.0075(2)	0.0043(2)	0.0078(3)	0	0.0053(2)	0
H(1)	0.0246(6)	0.0220(6)	0.0141(6)	0	0.0106(6)	0

Table 3b. Refined displacement parameters (Å^2) in the expression: $-2\pi^2[(ha^*)^2U_{11} + \ldots + 2hka^*b^*U_{12} + \ldots + 2klb^*c^*U_{23}]$, based on the data collected at 1070K. *Ueq* is defined as one third of the trace of the orthogonalised *Uij* tensor.

Site	U_{11}	U_{22}	U_{33}	U_{12}	U_{13}	U_{23}
CA(1)	0.041(4)	0.021(3)	0.037(4)	0	0.027(3)	0
CA(2)	0.032(3)	0.050(5)	0.025(4)	0	0.010(3)	0
SI(1)	0.008(2)	0.016(3)	0.017(3)	0	0.006(2)	0
SI(2)	0.011(2)	0.011(3)	0.015(3)	0	0.006(2)	0
SI(3)	0.013(2)	0.011(3)	0.013(3)	0	0.005(2)	0
M(1)	0.016(2)	0.006(3)	0.018(4)	-0.004(3)	0.006(2)	-0.002(4)
M(2)	0.012(2)	0.012(3)	0.017(3)	0.003(3)	0.005(2)	0.003(4)
M(3)	0.012(1)	0.025(2)	0.022(2)	0	0.006(1)	0
O(1)	0.017(1)	0.017(2)	0.032(2)	0.002(2)	0.012(1)	0.002(2)
O(2)	0.021(1)	0.021(2)	0.023(2)	-0.008(2)	0.009(1)	0.000(2)
O(3)	0.017(1)	0.013(2)	0.029(2)	-0.001(1)	-0.001(1)	-0.003(2)
O(4)	0.017(2)	0.013(3)	0.013(3)	0	0.001(2)	0
O(5)	0.018(2)	0.016(3)	0.019(3)	0	0.007(2)	0
O(6)	0.022(2)	0.018(3)	0.018(3)	0	0.015(2)	0
O(7)	0.012(2)	0.036(3)	0.022(3)	0	-0.003(2)	0
O(8)	0.021(2)	0.038(3)	0.036(3)	0	0.020(2)	0
O(9)	0.051(4)	0.055(4)	0.021(3)	0	0.024(3)	0
O(10)	0.024(2)	0.018(3)	0.027(3)	0	0.017(2)	0
H(1)	0.059(6)	0.043(7)	0.039(7)	0	0.026(6)	0

Table 4a. Principal mean square atomic displacements (U1,U2 and U3, x10^4 Å^2) and root-mean-square components (R1,R2 and R3, Å) based on the structural refinement at 298K.

Site	U1	U2	U3	R1	R2	R3	R1/R3
Ca(1)	123(3)	84(3)	58(6)	0.110	0.091	0.076	1.458
Ca(2)	161(3)	103(5)	68(4)	0.126	0.101	0.082	1.540
Si(1)	42(5)	35(2)	30(2)	0.065	0.059	0.054	1.194
Si(2)	46(3)	41(2)	38(4)	0.067	0.064	0.061	1.105
Si(3)	43(4)	36(2)	31(3)	0.065	0.060	0.055	1.189
M(1)	44(5)	37(5)	26(3)	0.066	0.060	0.051	1.297
M(2)	54(4)	42(5)	27(3)	0.073	0.064	0.052	1.416
M(3)	61(3)	53(2)	34(2)	0.077	0.072	0.058	1.331
O(1)	102(2)	57(2)	37(1)	0.101	0.075	0.060	1.672
O(2)	92(2)	76(2)	40(2)	0.095	0.087	0.063	1.526
O(3)	157(3)	47(1)	42(1)	0.125	0.068	0.064	1.944
O(4)	57(4)	46(2)	45(2)	0.075	0.067	0.067	1.119
O(5)	62(4)	51(2)	42(2)	0.079	0.071	0.064	1.220
O(6)	89(2)	44(2)	32(5)	0.094	0.066	0.057	1.658
O(7)	102(5)	99(2)	46(2)	0.100	0.099	0.067	1.489
O(8)	165(3)	144(3)	41(5)	0.128	0.119	0.064	2.000
O(9)	197(3)	183(3)	38(5)	0.140	0.135	0.061	2.274
O(10)	91(2)	43(2)	41(5)	0.095	0.066	0.064	1.492
H(1)	246(6)	220(6)	117(10)	0.156	0.148	0.108	1.451

Table 4b. Principal mean square atomic displacements (U1,U2 and U3, x10^4 Å^2) and root-mean-square components (R1,R2 and R3, Å) based on the structural refinement at 1070K.

Site	U1	U2	U3	R1	R2	R3	R1/R3
Ca(1)	458(30)	216(34)	215(69)	0.215	0.146	0.146	1.477
Ca(2)	497(51)	344(50)	249(33)	0.222	0.185	0.158	1.403
Si(1)	169(34)	161(31)	69(30)	0.130	0.126	0.083	1.573
Si(2)	154(35)	114(28)	100(31)	0.124	0.106	0.099	1.250
Si(3)	132(30)	125(37)	109(30)	0.115	0.112	0.104	1.099
M(1)	194(55)	171(27)	46(33)	0.138	0.132	0.068	2.038
M(2)	196(49)	148(43)	90(34)	0.139	0.122	0.095	1.470
M(3)	250(21)	233(30)	123(14)	0.157	0.152	0.111	1.419
O(1)	326(19)	182(25)	138(18)	0.181	0.134	0.117	1.546
O(2)	299(26)	232(17)	129(21)	0.172	0.153	0.113	1.522
O(3)	454(25)	155(15)	115(16)	0.212	0.125	0.107	1.977
O(4)	250(39)	127(25)	111(19)	0.157	0.112	0.106	1.484
O(5)	209(47)	179(17)	161(27)	0.144	0.134	0.126	1.136
O(6)	252(17)	183(26)	88(49)	0.159	0.135	0.093	1.716
O(7)	363(33)	362(40)	88(15)	0.189	0.189	0.094	2.015
O(8)	381(34)	374(27)	119(40)	0.195	0.194	0.108	1.794
O(9)	550(41)	516(33)	118(53)	0.234	0.228	0.108	2.157
O(10)	297(21)	185(27)	140(49)	0.174	0.136	0.118	1.475
H(1)	589(56)	428(71)	342(102)	0.243	0.206	0.184	1.318

Table 5a. Relevant bond distances and angles based on the diffraction data collected at 293K.

CA(1) - O(1) x 2	2.459(1) Å	O(1)-SI(1)-O(7)	111.83(5)°
CA(1) - O(3) x 2	2.329(1) Å	O(1)-SI(1)-O(9)	106.62(5)°
CA(1) - O(5)	2.552(2) Å	O(7)-SI(1)-O(9)	106.48(9)°
CA(1) - O(6)	2.855(3) Å	O(1)-SI(1)-O(1)	112.95(8)°
CA(1) - O(7)	2.295(2) Å		
CA(1) - O(9) x 2	3.002(2) Å	O(3)-SI(2)-O(3)	110.63(9)°
		O(3)-SI(2)-O(9)	107.20(6)°
		O(8)-SI(2)-O(9)	110.26(9)°
CA(2) - O(2) x 2	2.788(2) Å	O(3)-SI(2)-O(8)	110.72(6)°
CA(2) - O(2)'x 2	2.528(2) Å		
CA(2) - O(3) x 2	2.646(2) Å	O(2)-SI(3)-O(2)	107.05(8)°
CA(2) - O(7)	2.246(2) Å	O(2)-SI(3)-O(5)	111.72(6)°
CA(2) - O(10)	2.530(2) Å	O(2)-SI(3)-O(6)	112.43(6)°
		O(5)-SI(3)-O(6)	101.58(8)°
SI(1) - O(1) x 2	1.650(1) Å		
SI(1) - O(7)	1.570(2) Å	O(1)-AL(1)-O(4)	93.67(4)°
SI(1) - O(9)	1.634(2) Å	O(1)-AL(1)-O(4)'	86.33(4)°
<SI(1)-O>	1.626 Å	O(5)-AL(1)-O(4)	84.13(6)°
V(SI1)	2.197 Å^3	O(5)-AL(1)-O(4)'	95.87(6)°
M.P.Q.E.(SI1)	1.0032	O(5)-AL(1)-O(1)	89.22(5)°
		O(5)-AL(1)-O(1)'	90.78(5)°
SI(2) - O(3) x 2	1.617(1) Å		
SI(2) - O(8)	1.590(2) Å	O(3)-AL(2)-O(6)	90.29(5)°
SI(2) - O(9)	1.633(2) Å	O(3)-AL(2)-O(6)'	89.71(5)°
<SI(2)-O>	1.614 Å	O(3)-AL(2)-O(10)	88.29(5)°
V(SI2)	2.156 Å^3	O(3)-AL(2)-O(10)'	91.71(5)°
M.P.Q.E.(SI2)	1.0008	O(6)-AL(2)-O(10)	83.95(5)°
		O(6)-AL(2)-O(10)'	96.05(5)°
SI(3) - O(2) x 2	1.626(1) Å		
SI(3) - O(5)	1.665(2) Å	O(1)-AL(3)-O(1)	80.59(6)°
SI(3) - O(6)	1.641(1) Å	O(1)-AL(3)-O(4)	76.56(5)°
<SI(3)-O>	1.639 Å	O(1)-AL(3)-O(8)	101.74(5)°
V(SI3)	2.246 Å^3	O(2)-AL(3)-O(4)	93.18(4)°
M.P.Q.E.(SI3)	1.0048	O(2)-AL(3)-O(8)	88.29(5)°
		O(1)-AL(3)-O(2)	89.62(6)°
AL(1) - O(4) x 2	1.844(1) Å	O(2)-AL(3)-O(2)	98.75(7)°
AL(1) - O(1) x 2	1.938(2) Å	O(1)-Al(3)-O(2)	167.16(6)°
AL(1) - O(5) x 2	1.958(1) Å	O(4)-Al(3)-O(8)	177.74(7)°
<AL(1)-O>	1.913 Å		
V(Al1)	9.264 Å^3	SI(2)-O(9)-SI(1)	154.59(9)°
M.P.Q.E.(Al1)	1.0064		
AL(2) - O(3) x 2	1.854(2) Å		
AL(2) - O(6) x 2	1.926(1) Å		
AL(2) - O(10) x 2	1.870(1) Å		
<AL(2)-O>	1.883 Å		
V(Al2)	8.850 Å^3		
M.P.Q.E.(Al2)	1.0046		
AL(3) - O(1) x 2	2.225(1) Å		
AL(3) - O(2) x 2	1.986(2) Å		
AL(3) - O(4)	1.937(2) Å		
Al(3) - O(8)	1.855(2) Å		
<AL(3)-O>	2.036 Å		
V(Al3)	10.861 Å^3		
M.P.Q.E.(Al3)	1.0287		
O(10) - H(1)	0.9763(24) Å		
O(10) - H(1)*	0.9943 Å		
O(10)···O(2)	2.8221(17) Å		
O(10)···O(2)*	2.8223 Å		
H(1)···O(2)	2.5921(23) Å		
O(10) – H(1)···O2	93.3(1)°		
O(10)···O(4)	2.9318(22) Å		
O(10)···O(4)*	2.9321 Å		
H(1)···O(4)	1.9731(28) Å		
O(10) – H(1)···O4	166.7(2)°		

* Bond distance corrected for "riding motion" following Busing and Levy (1964).
M..P.Q.E. is the "mean polyhedral quadratic elongation" as defined by Robinson et al. (1971).

Table 5b. Relevant bond distances and angles based on the diffraction data collected at 1070K.

CA(1) – O(1) x 2	2.481(7) Å		O(1)-SI(1)-O(7)	111.5(3)°
CA(1) – O(3) x 2	2.356(7) Å		O(1)-SI(1)-O(9)	106.4(3)°
CA(1) – O(5)	2.581(9) Å		O(7)-SI(1)-O(9)	108.1(4)°
CA(1) – O(6)	2.840(9) Å		O(1)-SI(1)-O(1)	112.5(4)°
CA(1) – O(7)	2.317(8) Å			
CA(1) – O(9) x 2	3.016(6) Å		O(3)-SI(2)-O(3)	110.3(4)°
			O(3)-SI(2)-O(9)	107.3(3)°
			O(8)-SI(2)-O(9)	111.4(5)°
CA(2) – O(2) x 2	2.770(8) Å		O(3)-SI(2)-O(8)	110.3(3)°
CA(2) – O(2)'x 2	2.591(7) Å			
CA(2) – O(3) x 2	2.662(8) Å		O(2)-SI(3)-O(2)	107.2(4)°
CA(2) – O(7)	2.248(10) Å		O(2)-SI(3)-O(5)	111.3(3)°
CA(2) – O(10)	2.586(9) Å		O(2)-SI(3)-O(6)	112.5(3)°
			O(5)-SI(3)-O(6)	102.2(4)°
SI(1) – O(1) x 2	1.649(5) Å	[1.6581 Å]		
SI(1) – O(7)	1.558(8) Å	[1.5724 Å]	O(1)-AL(1)-O(4)	93.5(2)°
SI(1) – O(9)	1.621(8) Å	[1.6458 Å]	O(1)-AL(1)-O(4)'	86.5(2)°
<SI(1)-O>	1.619 Å	[1.6336 Å]	O(5)-AL(1)-O(4)	83.7(2)°
V(SI1)	2.171 Å^3		O(5)-AL(1)-O(4)'	96.3(2)°
M.P.Q.E.(SI1)	1.0028		O(5)-AL(1)-O(1)	89.2(2)°
			O(5)-AL(1)-O(1)'	90.8(2)°
SI(2) – O(3) x 2	1.623(6) Å	[1.6341 Å]		
SI(2) – O(8)	1.600(8) Å	[1.6159 Å]	O(3)-AL(2)-O(6)	90.0(2)°
SI(2) – O(9)	1.610(9) Å	[1.6350 Å]	O(3)-AL(2)-O(6)'	90.0(2)°
<SI(2)-O>	1.614 Å	[1.6298 Å]	O(3)-AL(2)-O(10)	88.4(2)°
V(SI2)	2.155 Å^3		O(3)-AL(2)-O(10)'	91.6(2)°
M.P.Q.E.(SI2)	1.0008		O(6)-AL(2)-O(10)	83.8(2)°
			O(6)-AL(2)-O(10)'	96.2(2)°
SI(3) – O(2) x 2	1.633(5) Å	[1.6403 Å]		
SI(3) – O(5)	1.654(8) Å	[1.6576 Å]	O(1)-AL(3)-O(1)	79.9(3)°
SI(3) – O(6)	1.649(7) Å	[1.6517 Å]	O(1)-AL(3)-O(4)	75.9(2)°
<SI(3)-O>	1.642 Å	[1.6475 Å]	O(1)-AL(3)-O(8)	100.1(2)°
V(SI3)	2.259 Å^3		O(2)-AL(3)-O(4)	93.9(2)°
M.P.Q.E.(SI3)	1.0041		O(2)-AL(3)-O(8)	89.6(2)°
			O(1)-AL(3)-O(2)	89.7(2)°
AL(1) – O(4) x 2	1.846(4) Å	[1.8476 Å]	O(2)-AL(3)-O(2)	99.4(3)°
AL(1) – O(1) x 2	1.948(3) Å	[1.9541 Å]	O(1)-Al(3)-O(2)	166.8(3)°
AL(1) – O(5) x 2	1.982(4) Å	[1.9850 Å]	O(4)-Al(3)-O(8)	174.7(3)°
<AL(1)-O>	1.925 Å	[1.9289 Å]		
V(Al1)	9.433 Å^3		SI(2)-O(9)-SI(1)	157.4(5)°
M.P.Q.E.(Al1)	1.0072			
AL(2) – O(3) x 2	1.859(3) Å	[1.8671 Å]		
AL(2) – O(6) x 2	1.951(4) Å	[1.9533 Å]		
AL(2) – O(10) x 2	1.876(4) Å	[1.8816 Å]		
<AL(2)-O>	1.895 Å	[1.9007 Å]		
V(Al2)	9.013 Å^3			
M.P.Q.E.(Al2)	1.0051			
AL(3) - O(1) x 2	2.289(5) Å	[2.2903 Å]		
AL(3) - O(2) x 2	2.001(5) Å	[2.0025 Å]		
AL(3) - O(4)	1.915(6) Å	[1.9118 Å]		
Al(3) - O(8)	1.839(6) Å	[1.8463 Å]		
<AL(3)-O>	2.056 Å	[2.0573 Å]		
V(Al3)	11.160 Å^3			
M.P.Q.E.(Al3)	1.0326			
O(10) - H(1)	0.951(16) Å			
O(10) - H(1)*	0.9826 Å			
O(10)···O(2)	2.863(8) Å			
O(10)···O(2)*	2.8643 Å			
H(1)···O(2)	2.595(12) Å			
O(10) – H(1)···O2	96.5(2)°			
O(10)···O(4)	3.005(10) Å			
O(10)···O(4)*	3.0072 Å			
H(1)···O(4)	2.067(16) Å			
O(10) – H(1)···O4	169.1(12)°			

* Bond distance corrected for "riding motion" following Busing and Levy (1964).
M..P.Q.E. is the "mean polyhedral quadratic elongation" as defined by Robinson et al. (1971).
In the squared brackets: bond distances corrected for "rigid body motions" following Downs et al. (1992) and Downs (2000).

Fig. 1 The crystal structure of epidote viewed down [100] (*above*) and [100] (*below*), respectively, based on the atomic coordinates refined in this study at 298K (thermal ellipsoid probability factor: 50%)

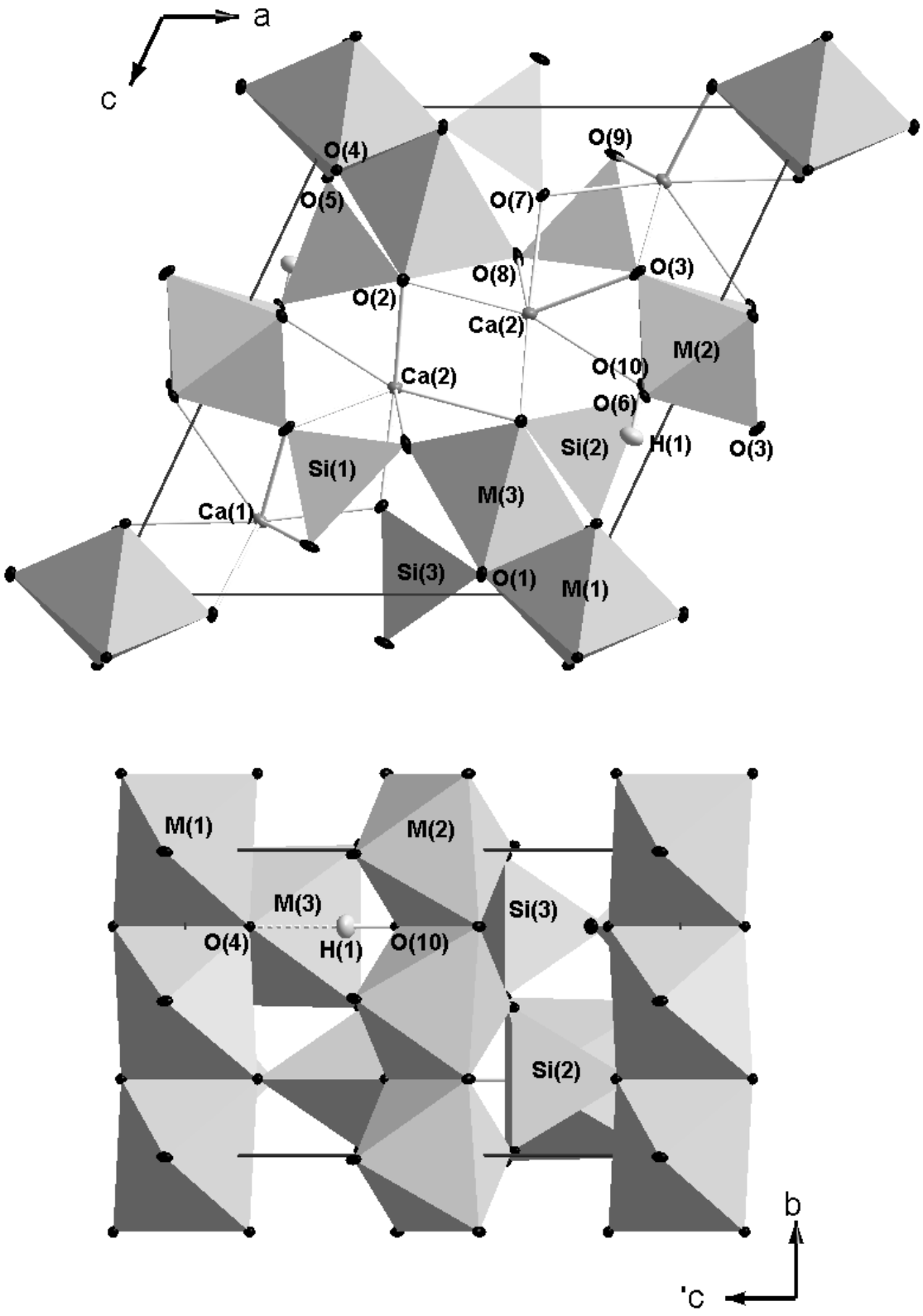

Fig. 2 Difference Fourier maps of the nuclear density (fm/Å^3) of epidote (at 298K) at *y*=1/4, (*above*) before and (*below*) after the assignment of the H-sites. One intense negative residual peaks at *x*~0.05 and *z*~0.32 is evident before the assignment of the proton site. (*Notes*: the gray scale is different for the two maps; map orientation: *x* positive to the right).

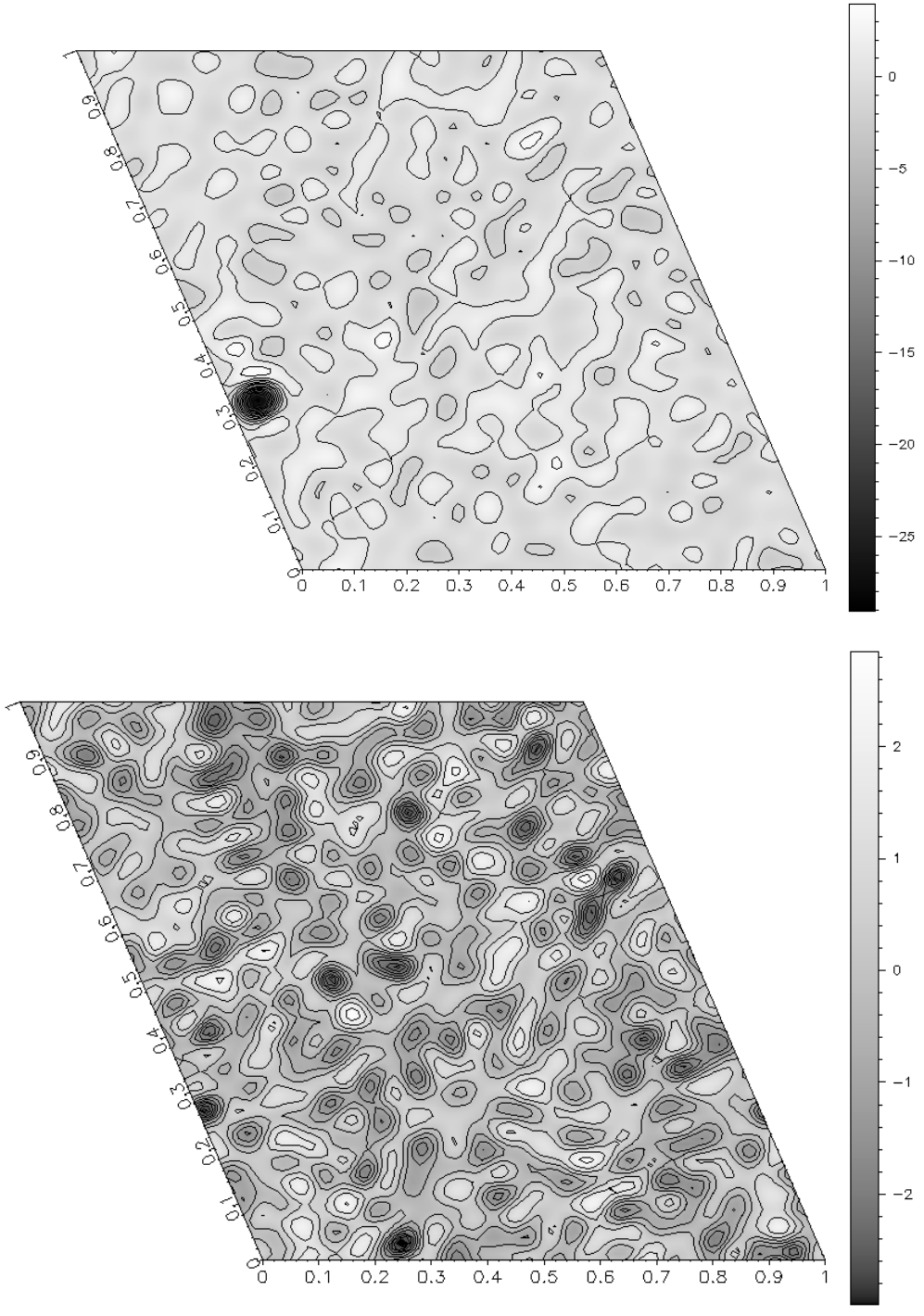

Fig. 3 (*Above*) Crystal structure of epidote based on the refinement at 298K (*left side*) and at 1070K (*right side*), respectively. Atomic site labels are in Figure 1. Thermal ellipsoid probability factor: 99%. (*Below*) Configuration of the hydrogen bond in epidote at 298K (*left side*) and 1070K (*right side*), respectively.